Temperature induced structural changes of tetrahydrofuran clathrate and of the liquid water/tetrahydrofuran mixture

ARTICLE *in* THE JOURNAL OF PHYSICAL CHEMISTRY C · NOVEMBER 2011

Impact Factor: 4.77

THE JOURNAL OF PHYSICAL CHEMISTRY C

ARTICLE

pubs.acs.org/JPCC

Temperature-Induced Structural Changes of Tetrahydrofuran Clathrate and of the Liquid Water/Tetrahydrofuran Mixture

Felix Lehmkühler,*[,†,∥] Arto Sakko,[‡] Ingo Steinke,[†,∥] Christian Sternemann,[†] Mikko Hakala,[‡] Christoph J. Sahle,[†] Thomas Buslaps,[§] Laura Simonelli,[§] Szabolcs Galambosi,[‡] Michael Paulus,[†] Tuomas Pylkkänen,[‡] Metin Tolan,[†] and Keijo Hämäläinen[‡]

[†]TU Dortmund, Fakultät Physik/DELTA, 44221 Dortmund, Germany

[‡]Department of Physics, POB 64, FI-00014 University of Helsinki, Helsinki, Finland

[§]European Synchrotron Radiation Facility, Boite Postale 220, 38043 Grenoble cedex 9, France

ABSTRACT: We present two complementary inelastic X-ray scattering studies on the structure of tetrahydrofuran (THF) clathrate hydrate and the supercooled stoichiometric liquid mixture of water and THF. Compton scattering experiments of the liquid mixture show that formation of hydrate precursors is unlikely. By comparing experimental spectra of THF hydrate and water/THF mixtures at temperatures above 250 K with density functional theory calculations, structural changes that manifest in OH bond length changes are observed. X-ray Raman scattering measurements of the oxygen K-edge in the same temperature range corroborate these results. The experimental results of THF hydrate at temperatures between 20 and 244 K can be modeled best by assuming thermal expansion only. Therefore, dependency on the system's temperature different structural behavior of THF hydrate is reported.

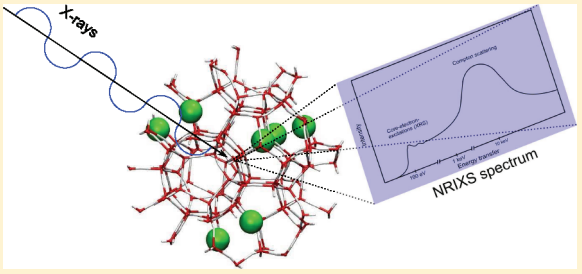

INTRODUCTION

Clathrate hydrates are important materials for present day science and technology because of their potential applications and relevance in environmental processes. These ice-like compounds consisting of water cages in which guest molecules are enclosed[1,2] are potential materials for gas storage at moderate pressures and temperatures, for example, H_2 for fuel cell applications.[3] In recent years, it has been shown that the addition of tetrahydrofuran (THF) allows H_2 storage at moderate pressures, providing a safe and applicable gas storage material.[4,5]

Pure THF hydrate (structure sII) has been part of many studies because it can be synthesized easily at temperatures below 277 K at atmospheric pressure.[6] As with other oxygen-containing guests, THF hydrate exhibits some anomalies near its melting point, for example, abnormal heat capacity[7,8] and thermal expansivity.[9] Recent molecular dynamics (MD) simulations reported the formation of hydrogen bonds between the water cage and the oxygen atom of guest molecules that occurs in particular in THF hydrate.[10] However, experimental X-ray studies did not find any indication for such processes in THF hydrate.[11,12] Therefore, most of the abnormal characteristics of THF hydrate remain unsolved. In former studies, we found indications for a structural change in THF hydrate above $T = 250$ K and were able to connect the anomaly of the hydrate's configurational heat capacity with changes in its intramolecular structure, in particular, a change in the OH bond length of the water molecules.[12,13] Nevertheless, the nature of this structural rearrangement is still not understood. Similarly, despite an increasing number of studies during recent years, the formation process of clathrate hydrates from a liquid mixture is still under discussion. Many MD simulations that have been performed for methane or CO_2 hydrate[1,14−18] show a variety of different nucleation pathways. These can be divided into processes involving hydrate precursors, that is, cage structures consisting of water and guest molecules under supercooled conditions, and in processes that suggest a spontaneous nucleation without any precursor structures. In contrast, experimental studies of the hydrate formation process on molecular length scales from the liquid phase are rare. By studying the water−CO_2 interface with X-ray reflectivity and diffraction, we found no indications for hydrate precursors.[19] Furthermore, by comparing the oxygen K-edge of a liquid water/THF mixture, no indications for hydrate precursors in a supercooled sample were observed.[13]

Nonresonant inelastic X-ray scattering (NRIXS) is a powerful tool to study the sample's electronic structure.[20] The energy and momentum transfers of the inelastically scattered photons $\hbar\omega$ and $\hbar\mathbf{q}$, respectively, can be varied independently. In the regime of large momentum and energy transfers, that is, Compton scattering, this method is very sensitive to changes of the intra- and intermolecular structures of the sample.[21] Hence, Compton scattering is frequently used to study hydrogen bonded systems with respect to, for example, bond stretching, bending and formation,

Received: July 22, 2011
Revised: September 12, 2011
Published: September 13, 2011

and phase transitions.[22−28] Recently, studies on the guest−host interaction and structure in hydrates[12,29] and the isostructural silicon clathrate[30] were also performed. Probing NRIXS with the energy transfer close to the binding energy of core electrons, one can study the inner-shell excitations. This method (X-ray Raman scattering, XRS) enables the study of soft X-ray absorption edges with bulk sensitivity using hard X-rays.[20,31−34] In the limit of small wave vector transfers $q = |\mathbf{q}|$ XRS provides similar information to X-ray absorption spectroscopy, whereas the unique possibility to vary q in XRS experiments also allows access to nondipole transitions. XRS has become a standard tool to study coordination and ordering in water and ice systems.[35−38] In particular, changes in the sample's local structure in the first and second coordination shells manifest in modifications of the oxygen K-edge in these systems. Here a higher degree of order, for example, ice compared with water, results in a shift of specific spectral features. Hence this technique is well-suited for studying structural properties of amorphous systems, in particular liquids.

In recent studies, we investigated the formation process of THF hydrate by means of XRS[13] and the structural change of THF hydrate at temperatures between 93 and 275 K using Compton scattering.[12] By comparing XRS spectra of a supercooled and a nonsupercooled mixture of water and THF, no indications for hydrate precursors at supercooled conditions were found. Furthermore, the spectra of the hydrate between 254 and 274 K exhibit differences that were interpreted as increased structural order in the hydrate at lower temperatures. Compton scattering experiments suggest different OH bond lengths of the water molecules forming the hydrate cage. In contrast, at temperatures below 254 K the changes in the Compton profile could be explained by thermal expansion. Nevertheless, a full knowledge of high-temperature processes, THF hydrate formation, and structural changes in the hydrate is still missing.

In this Article, we extend those works and report on the formation of THF hydrate by means of X-ray Compton scattering and XRS for temperatures between 20 and 275 K. To expand the previous XRS study to inter- and intramolecular local structures, the hydrate formation is investigated by comparing experimental Compton profiles of a liquid water/THF mixture at different temperatures and with profiles of the hydrate. The formation of hydrate precursors would be visible as changes of the local structure and can therefore be measured by Compton scattering experiments. A comparison of calculated Compton profiles within the framework of density functional theory (DFT) will facilitate interpretation of the data. The microscopic structure of the liquid mixture at supercooled conditions appears to be similar to that in the nonsupercooled state so that the formation of hydrate precursors is unlikely. To expand the findings of the previous Compton scattering experiment and to gain more information on structural changes in THF hydrate, we measure oxygen K-edges of THF hydrate at temperatures between 20 and 275 K by XRS. Below 244 K, the spectral change can be shown to reflect the normal thermal expansion, but between 244 and 275 K, the situation is more complicated and the data suggest an increase in order with decreasing temperature. The DFT calculations connect this effect to changing OH bond lengths.

EXPERIMENTAL AND COMPUTATIONAL DETAILS

Compton Scattering. The measured quantity in Compton scattering experiments is the double differential scattering cross section. Within the impulse approximation,[21] it is directly proportional to the isotropic Compton profile

$$J(p_q) = \frac{1}{2}\int d\Omega \int_{|p_q|}^{\infty} p\rho(\mathbf{p})\, \mathrm{d}p \qquad (1)$$

where p_q denotes a scalar electron momentum variable and $\rho(\mathbf{p})$ is the electron momentum density with the electron momentum $\mathbf{p}$. Compton profiles are very sensitive to changes of the electron wave functions and thereby also to changes of the local structure of the sample.

The experimental Compton profiles were measured at beamline ID15B of the European Synchrotron Radiation Facility (ESRF).[39] The energy of the incident X-rays was 86.89 keV, and the scattered intensity was measured by a 13-element germanium solid-state detector at a scattering angle of ∼160°. The beam size was chosen to be 0.1 × 0.3 mm^2 ($v \times h$). The momentum resolution was approximately $\Delta p_q = 0.6$ atomic units (a.u.) of momentum at the Compton peak, that is, $p_q = 0$ a.u. To achieve a constant incident photon flux at the sample that is necessary to guarantee the required detector stability, we used an absorber feedback system. The liquid mixture of THF (Sigma Aldrich, purity >99.9%) and water (Millipore) with a stoichiometry of 1:17 fraction (19 wt % THF) that corresponds to a full occupation of all large cages of the sII structure[1] was filled in the sample cell.[40] The mixture was measured at 299 K, 287 K, and at the supercooled temperature of 275 K. Afterward, the sample was mixed to initiate the macroscopic growth of THF hydrate, verified by X-ray diffraction. Then, spectra of the hydrate were measured at 275, 265, and 253 K. Each temperature was measured for ∼8 h. To check the data for consistency, spectra were saved every 10 min and compared to detect deviations larger than the statistical accuracy. Altogether, the statistical accuracy was better than 0.03% units at $p_q = 0$ a.u. within a 0.03 a.u. momentum bin. The raw data were corrected for absorption before converting to momentum scale using the relativistic cross section correction.[41] Finally, a correction for multiple scattering was performed, and the positive and negative momentum sides of the Compton profiles were averaged. To compare the Compton profiles of the different temperatures and phases, only Compton profile differences are discussed here. This serves to cancel out any systematic errors in both experiment and theory.

X-ray Raman Scattering. The experimental XRS spectra were measured at beamline ID16 of ESRF. The multiple-analyzer crystal spectrometer for nonresonant inelastic X-ray scattering[42] was used at a fixed analyzer energy of 9.69 keV. By varying the incident energy, various energy transfers in the vicinity of the oxygen K-edge were accessed. The scattered and analyzed X-rays were detected by a Maxipix 2D detector. With bent Si(660) analyzer crystals, an overall energy resolution of $\Delta E \approx 0.55$ eV was achieved. A sample cell similar to the one previously described[40] was adapted to a cryostat setup. The stoichiometric 17:1 (water/THF) mixture was filled inside the cell, cooled to 275 K, and stirred to initiate the hydrate growth. After the complete growth of THF hydrate had been confirmed by X-ray diffraction, the measurement was started at 275 K. XRS spectra were measured simultaneously for five scattering angles between θ = 127 and 153°, corresponding to momentum transfers q = 9.01 to 9.83 Å^{-1}. In contrast with absorption spectroscopy, such high momentum transfers enable one to detect also nondipole transitions. For instance, in the case of water systems, $s-s$

transitions give a significant contribution to the preedge region at these momentum transfers.[38] The oxygen K-edge was measured in the energy transfer region of 530−550 eV for ∼4 h at each temperature. To avoid radiation damage in the sample,[13,37] an unfocused beam with a size of 1 × 3 mm^2 ($v \times h$) was used together with a specific sample movement. XRS spectra were measured for 274, 264, 254, 244, 150, 50, and 20 K. The raw data were analyzed following the procedure described in ref 43. Because the q dependence of the XRS spectra is very weak within the probed momentum transfer range, the spectra for all scattering angles were summed to increase the statistical accuracy.

Calculations. Calculating the Compton profile requires a structural model (atomic coordinates) for the system being studied. For liquids, a typical approach for obtaining them is to carry out MD simulations and extract instantaneous structures from the simulation snapshots. Compton profiles of these model structures can be calculated using, for example, DFT. However, in typical MD simulations, the number of atoms is several thousand, which is beyond the capabilities of the present day computational methods for electronic structure calculations. Instead, one can extract N small clusters from the full simulation, each containing 10−100 molecules that lie within a sphere of radius R from a randomly chosen point in the simulation cell. Their averaged Compton profile represents the full profile

$$J_{\mathrm{tot}}(p_q) \approx \frac{1}{N}\sum_{k=1}^{N} J_k(p_q) \tag{2}$$

where $J_k(p_q)$ are normalized according to the number of electrons in the small clusters. For liquids that contain various different molecules, the averaged Compton profile does not generally fulfill the stoichiometry condition of the system. Therefore, we replace the pure Compton profile in eq 2 by a weighted average

$$J_{\mathrm{tot}}(p_q) \approx \sum_{k=1}^{N} w_k J_k(p_q) \tag{3}$$

where the weights w_k depend on the number of different molecules in each cluster and are chosen in such a way that the appropriate stoichiometry condition is fulfilled. In this work, the weights are determined by the two equations

$$\sum_{j=1}^{N} w_j N_j^{\mathrm{THF}} = 1, \quad \sum_{j=1}^{N} w_j N_j^{\mathrm{H_2O}} = 17 \tag{4}$$

where N_j^{THF} and $N_j^{\mathrm{H_2O}}$ are the numbers of THF and H_2O molecules in the jth cluster, respectively. In a general case, the relative numbers of different molecules in the mixture form the vector $\mathbf{s}$ and the equation for the weights is $\mathbf{Nw} = \mathbf{s}$, where N_{ij} is the number of molecules of species i in the cluster j.

Another feature whose effect has to be carefully tested in the difference profile calculations is the finite size of the extracted clusters. Some of the molecules in the clusters are in the surface region and thereby have unrealistic chemical surroundings. Fortunately, these effects usually cancel out in the difference profiles, especially if the compared structures are sufficiently similar. To obtain reliable difference Compton profiles for comparison with experimental results, one should increase the size of the extracted clusters until the results are converged within required accuracy. Nevertheless, the convergence can be slow and some uncertainties in the calculated Compton profile remain. The calculation can be used for the interpretation of the experimental data only if these errors are relatively small compared with the structural effects.

The computational method and its details (computer code,[23,44] basis sets, exchange-correlation potential, etc.) used for the Compton profile calculations in this work are the same as those used in ref 12. The profile of the liquid was calculated from MD simulation snapshots[13] using eqs 3 and 4. The cutoff radius for generating the small clusters was 5.0 Å and 100 clusters were used. The structural model for hydrate profile calculation was generated using experimental neutron diffraction data.[45] Compton profiles were calculated for three different structures:

$J_1(p_q)$: a large (28× H_2O) empty cage.
$J_2(p_q)$: a large (28× H_2O) cage with a THF molecule inside.
$J_3(p_q)$: a small (20× H_2O) empty cage.

In addition, the Compton profile of an isolated THF molecule ($J_{\mathrm{THF}}(p_q)$) was calculated. The contribution of the interaction of one THF molecule with its surroundings is then $J_{\mathrm{int}}(p_q) = J_2(p_q) - J_1(p_q) + J_{\mathrm{THF}}(p_q)$. We accounted for the basis set superposition error by including the basis set of a ghost THF molecule in the calculation of $J_1(p_q)$. Similarly, the Compton profile from the cages is

$$J_{\mathrm{cages}}(p_q) = \frac{2 \times J_3(p_q) + 1 \times J_1(p_q)}{2 \times 20 + 1 \times 28} \tag{5}$$

where the coefficients 2 and 1 originate from the 2:1 stoichiometry of small and large cages in the hydrate phase. This profile is normalized to the number of electrons in a single H_2O molecule (10), that is, $\int_0^\infty dp_q J_{\mathrm{cages}}(p_q) = 10$. The total hydrate profile is then

$$J_{\mathrm{hyd}}(p_q) = 17 \times J_{\mathrm{cages}}(p_q) + 1 \times J_{\mathrm{THF}}(p_q) + J_{\mathrm{int}}(p_q) \tag{6}$$

where $J_{\mathrm{THF}}(p_q)$ is normalized to the number of electrons in the molecule (40). We thus neglect the surface effects in both liquid and hydrate phases. We also tested the influence of the motion of THF molecules in the cage by slightly displacing the THF molecule. This only yields minor effects in the liquid-hydrate difference profiles, and the effect was therefore omitted.

X-ray Raman scattering calculations were carried out using the same DFT-based[44,46] framework as described in ref 13 and are only briefly described here. The liquid phase calculations were based on the structures from MD snapshots, with 135 extracted clusters and a cutoff radius of 5.5 Å. The structural model for hydrate phase calculations was obtained from neutron diffraction data,[45] similar to the Compton scattering case. However, single cage structures are not sufficient here for proper calculations because water molecules are not bonded to the molecules in surrounding cages; therefore, their XRS spectra do not reflect the actual local structure of the hydrate. In this case, several cages were combined to form a larger structure. Then, a set of oxygen-centered clusters with realistic chemical surroundings could be extracted. The XRS spectra of each 18 clusters were averaged to obtain the total oxygen K-edge spectrum.

RESULTS AND DISCUSSION

Compton Scattering. *Cage Occupancy.* As mentioned above, in our previous study, we found some intriguing structural changes of THF hydrate taking place at the temperature region above 250 K. As a possible explanation to those findings, we consider here the possibility of a modified hydrate structure where some THF molecules have escaped from the cage. The occurrence of these unenclosed THF molecules is suggested by

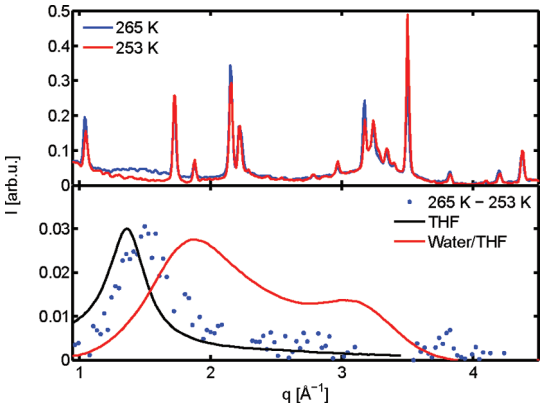

Figure 1. Top: Diffraction patterns of THF hydrate at 265 and 253 K. Bottom: Difference of diffraction patterns of THF hydrate compared with pure liquid THF and the stoichiometric water/THF mixture. The Bragg reflections are cut out from the data.

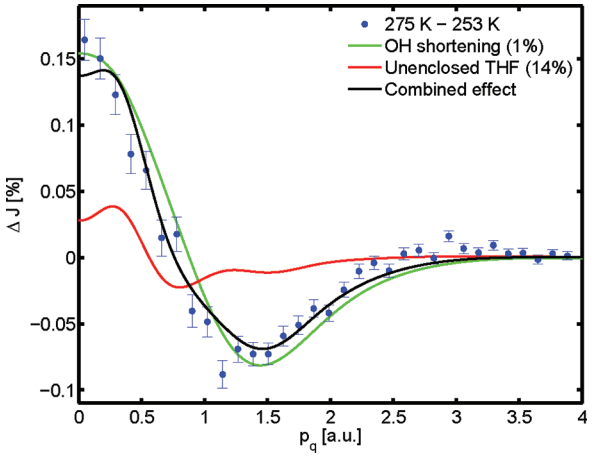

Figure 2. Experimental and computational Compton profile differences of THF hydrate. The combined effect yields (0.71 ± 0.10)% OH bond length shortening and (14 ±3)% unenclosed THF molecules.

X-ray diffraction patterns from THF hydrate above 253 K where a weak broad feature can be observed near the position of the structure peak originating from liquid THF; see Figure 1. This feature vanishes at 253 K, suggesting the existence of unbound THF molecules at temperatures of 265 and 275 K. However, compared with liquid THF, the position of the diffraction peak is shifted. This may be caused by unenclosed THF molecules either in an occurrence of a highly concentrated liquid THF/water mixture or confined between domains of the water cage lattice structure.

To see how this structural model would affect the experimental spectra, we performed additional DFT calculations from liquid THF structures and empty hydrate cages. To determine the fraction of THF molecules that are not enclosed in cages, we fitted a superposition of such calculated Compton profiles together with profiles from THF hydrate allowing a variation of the OH bond length to the experimental Compton profile difference between the hydrate at 275 and 253 K. (See Figure 2.) The fit considering both the change of OH bond length and the occurrence of unenclosed THF molecules yields a value of (0.71 ± 0.10)% shortening of the OH bond length together with an amount of (14 ± 3)% of the THF molecules that are not

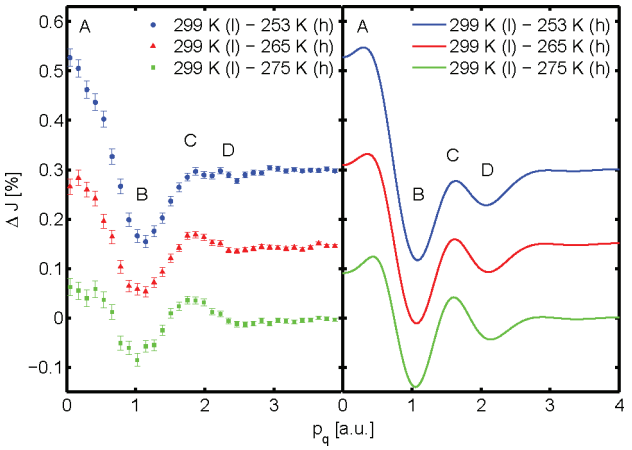

Figure 3. Experimental (left) and calculated (right) Compton profile differences between a liquid water/THF mixture (l) and THF hydrate (h) at different temperatures. The calculated profiles also take into account the effect of unenclosed THF molecules. Data and calculations are shifted vertically for clarity.

enclosed in large cages. In contrast, neglecting unenclosed THF molecules a change of OH bond length of 1% between 275 and 253 K was reported.[12] As can be seen from Figure 2, the combination of the OH bond length change and the occurrence of unenclosed THF molecules provides the best explanation of the data. Therefore, we conclude, that the OH bond length is reduced during cooling, accompanied by a decrease in the amount of unenclosed THF molecules. This contraction of the OH bond may be originated by a larger volume of the occupied cage compared with the empty cage, resulting in a weakening of the hydrogen bonds and consequently smaller OH bond lengths.[47] It is important to note that both experiment and calculation yield only information on the averaged change of bond length; the OH length of a particular molecule cannot be estimated. Furthermore, OH bond lengths in a highly concentrated liquid mixture of water and THF may also differ significantly as a function of water content;[48] however, compared with the number of water molecules forming the cage structure, the number of water molecules in such a mixture is low, if not zero. Because the differences below 253 K are weak and can be fully understood with the change of the lattice constant with temperature, the hydrate cage is taken to be fully occupied at 253 K.

THF Hydrate Formation. Figure 3 shows liquid-hydrate Compton profile differences. In general, the liquid-hydrate differences resemble the Compton differences of water and ice,[49] but a pronounced dependence on hydrate temperature is visible. The Compton differences show the same oscillatory features as the water/ice system, which are typical for changes in the water hydrogen bond system, that is, a maximum at $p_q = 0$ a.u. (A), a minimum at $p_q \approx 1$ a.u. (B), and a second maximum at $p_q \approx 1.8$ a.u. (C). However, differing from ice, the amplitude of the minimum is only approximately half of the value found in the water-ice difference. The amplitude of the second maximum is generally smaller and decreases with decreasing temperature. These findings can be understood as special features of the hydrate structure and of the guest molecule. In Figure 3 (right), Compton profile differences computed in the framework of DFT are shown. To decrease the influence of different models used (MD for the liquid phase and neutron scattering data for the hydrate phase), we scaled all OH and OO bond lengths of the hydrate structure

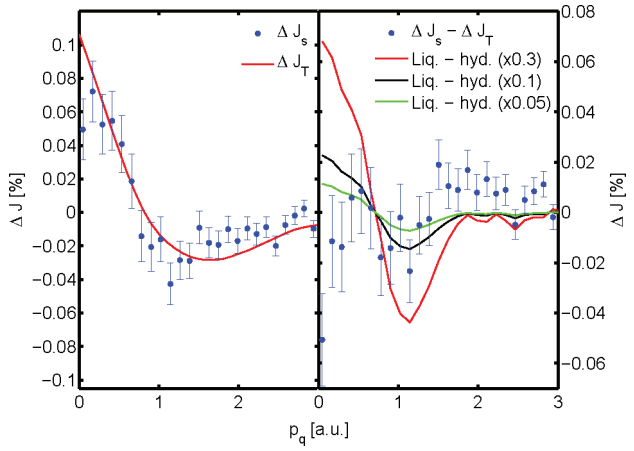

Figure 4. Left: Compton profile differences of the stoichiometric water/THF mixture between 299 and 275 K ($\Delta J_s = J(299\text{K}) - J(275\text{K})$) compared with the mixture between 299 and 287 K (smoothed data curve). The latter is scaled by a factor of 2 to model the temperature effect $\Delta J_T = (J(299\text{K}) - J(287\text{K})) \times 2$ between 299 and 275 K. Right: ΔJ_s with temperature effect ΔJ_T subtracted compared with scaled experimental liquid - hydrate differences between 299 and 253 K. (See Figure 3.)

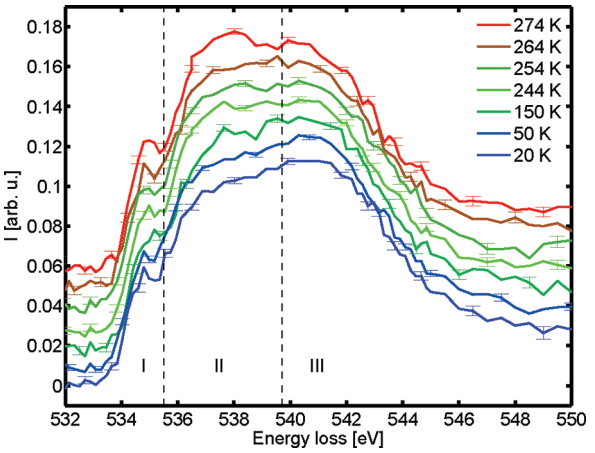

Figure 5. Oxygen K-edge of THF hydrate at different temperatures. The spectra are subdivided in three parts: preedge (I), main edge (II), and postedge (III) region. Spectra are shifted vertically for clarity.

in such a way that the difference profile fits the experimental data. Variations of these bond lengths affect mainly the amplitude of the profile differences. For 265 and 275 K, the calculations include unenclosed THF molecules of 7 and 14%, respectively. In Figure 3, the features A and B are well-reproduced by the experimental data (with exception of the shape close to $p_q = 0$ a.u.). In contrast, the maximum C and, in particular, the minimum D are either only slightly expressed or cannot be resolved. However, the variation of spectral features as a function of temperature clearly shows the same trend in both experiment and computation. The deviations from the experimental data can be attributed to the lack of cluster surface effects, possible inaccuracies of the structural models, and the shortcomings of DFT (especially near $p_q = 0$, see feature A).[50] The change of the difference for various THF hydrate temperatures, as shown in Figure 3, reflects well the variation of the OH bond length in THF hydrate, as previously observed.[12]

In addition to the comparison of Compton profiles of the liquid and hydrate phase, changes in the Compton profiles of the liquid phase only were also studied to find indications of hydrate precursors. The measured Compton profile difference of a stoichiometric (17:1 water/THF) liquid mixture at 299 and 275 K (ΔJ_s) is shown in Figure 4 (left). The comparison with a scaled difference between 299 and 287 K, where no hydrate precursors can occur, yields no considerable differences between the data sets. The latter difference is a measure of the bare temperature effect ΔJ_T in the water/THF mixture. In Figure 4 (right), ΔJ_T is subtracted from the ΔJ_s, which represents a measure of structural changes occurring in the supercooled phase and should indicate signatures of hydrate precursors if they appear. Hydrate precursors have a similar local structure as macroscopic hydrate,[1] in particular, on short length scales that are accessible by Compton scattering. We assume that the formation of hydrate precursors would result in profile differences similar to liquid-hydrate differences, although with smaller amplitudes. This can be modeled by scaled liquid-hydrate differences between 299 and 254 K where the hydrate is fully formed from Figure 3. With this scaling, we estimate an upper limit for the fraction of molecules forming THF hydrate precursors in the liquid water/THF mixture below 10%. Therefore, occurrence of hydrate precursors is unlikely within the limits of our experiment.

X-ray Raman Scattering. The oxygen K-edges of THF hydrate at different temperatures are shown in Figure 5. Following previous studies,[13,37] the oxygen K-edge is subdivided in three regions: a preedge (I), the main edge (II), and a postedge (III) region. The magnitude of spectral changes in the preedge region is on the order of the statistical accuracy for all temperatures. Furthermore, because the influences of the sample's local structure on the preedge region are not yet fully understood,[35,37,38,51] this region will not be discussed in this work. With decreasing temperature, a shift of spectral weight from region II to III is observable. According to previous publications, this is connected with an increase in order[37] or an increased distance of the second coordination shell.[38] In agreement with the Compton data, the spectral change is more pronounced at temperatures above 244 K, where a temperature step of 10 K yields significantly different edge shapes, whereas at low temperatures only small deviations can be found. Therefore, we conclude that the structure of THF hydrate is more disordered at high temperatures, whereas the order increases at lower temperatures.

To interpret the differences of the XRS spectra for various temperatures more quantitatively, the overall spectral change is demonstrated by the main-to-postedge ratio of the edges; see Figure 6. The position of the main edge was chosen to $E_{\text{main}} = (538 \pm 0.5)$ eV, and the postedge is found at $E_{\text{post}} = (540.7 \pm 0.5)$ eV. In addition, integrals of the absolute value of the spectral differences are calculated with respect to the spectrum measured at 20 K, shown as inset in Figure 6. The integration limits were chosen to be $a = 536$ eV and $b = 545$ eV. Both the area $\Delta = \int_a^b |I_1 - I_2| \, dE$ and the main-to-postedge ratio reflect the degree of spectral and thus structural change in THF hydrate. Two different temperature ranges are visible: below $T \approx 250$ K, where a weak change of the spectra is observed, and above $T \approx 250$ K. These ranges are the same that were identified in the Compton scattering study.[12] The weak changes below $T \approx 250$ K were explained by thermal expansion only, whereas at high temperatures the OH bond length change discussed above dominates. Therefore, the similarity of both the XRS and the Compton scattering data shown in ref 12 supports the thermal anomalies of THF hydrate, as previously presented.

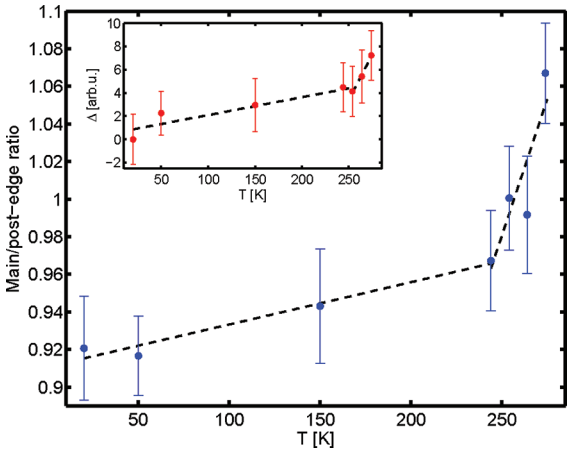

Figure 6. Main-to-postedge ratio as a function of temperature. Inset: Integrals of the absolute values of the XRS spectra differences with respect to the spectrum at 20 K. The black dashed lines represent guide to the eyes for both temperature ranges.

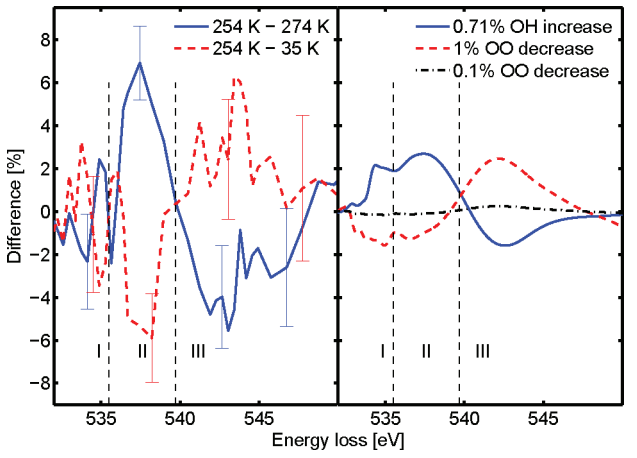

Figure 7. Differences of the experimental (left) and computed (right) XRS spectra. The spectra are subdivided in three parts: preedge (I), main edge (II), and postedge (III) region.

To discuss the changes of the XRS spectra in more detail, DFT calculations of different hydrate structures were performed. Differences of calculated spectra compared with experimental differences with respect to the spectrum at 254 K are shown in Figure 7. Because of the similarity of the edges at 20 and 50 K, they were averaged to increase the statistical accuracy and labeled with the mean value of 35 K. The same was done for 254 K, where the spectra at 244, 254, and 264 K from Figure 5 were averaged. XRS spectra were calculated for structures that were equivalent to the original hydrate structures[45] but where the OO or the OH bond lengths were scaled to model the temperature effect due to lattice expansion (OO) and the OH bond length stretch at higher temperatures, respectively. The same approach was previously used for the Compton profile calculations.[12] The accuracy of such calculations depends on the applicability of the computational method to simulate core-excited state potential energy surfaces. Recent work[52] suggests that good results will be obtained with the method used in this work.

The difference between experimental spectra of 35 and 254 K shows similar features as the computational results for an increase in the OO bond length of 1% that corresponds to the thermal expansion of the sample.[45] A similar comparison was successfully performed to model the Compton profile differences of THF hydrate.[12] However, in XRS, the overall shape in regions II and III but not the amplitude could be accurately modeled. One possible reason for the difference is the varying position of the THF molecule inside the cage. Such motions have been studied in previous MD simulations and nuclear magnetic resonance spectroscopy studies. According to those studies, the guest molecules freeze in energetically preferred positions only below at least 100 K.[53,54] The motion at higher temperatures could be detected in high-resolution XRS experiments, but our calculations were not affected by variations of the position of the THF molecule inside the cage.

In general, the increase in the OH bond length of 0.71% for $\Delta T \approx 20$ K, as suggested from the Compton scattering data, reflects the overall shape of the difference of XRS spectra. We also performed DFT calculations of other structures to test the effect of cage distortions, that is, ellipsoidal-shaped cages, and various off-center positions of the THF molecule. No significant changes in the oxygen K-edge were found because local variations, for example, due to different THF−water distances, average out. The change of the OH bond length is therefore the most likely explanation of the data. However, owing to the accuracy of the experiment, other structural changes that may affect the shape of the edge cannot fully be ruled out. The effect from the thermal expansion of 0.1% change in the OO distance per 20 K (Figure 7) can obviously be neglected for these temperatures.

SUMMARY

In summary, we have presented two separate and complementary inelastic X-ray scattering studies on THF hydrate. Using computational methods, we were able to interpret the experimental data in terms of structural properties and found new information on the structure of the supercooled liquid mixture. In agreement with previous results, a stochastic hydrate formation process is preferred where no precursor structures are formed when the supercooled region is reached.

At temperatures between 20 and 250 K, the data reflect an increase in the OO distance due to thermal expansion. Interesting effects were found between 250 and 275 K. The Compton profiles can be modeled assuming a change of the OH bond length in THF hydrate possibly accompanied by a decrease in the fraction of unenclosed THF molecules. The change of OH bond length may be originated in a weakening of the hydrogen bond in unoccupied water cages. Experimental and computed XRS spectra support these findings. The good agreement between theory and experiment validates our approach in obtaining local structural information by combining these two methods. Both Compton and XRS are sensitive to the same effects. Future high-resolution experiments could provide structural information about, for example, guest molecule freezing at low temperatures.

AUTHOR INFORMATION

Corresponding Author

*E-mail: felix.lehmkuehler@desy.de.

Present Addresses

[||]Deutsches Elektronen Synchrotron (DESY), Notkestr. 85, 22607 Hamburg, Germany.

■ ACKNOWLEDGMENT

We thank Federica Venturini and Simo Huotari for support during the beamtimes, Dietmar Paschek for providing MD snapshots and discussions, and Veijo Honkimäki for providing the program for multiple scattering calculations. The ESRF is gratefully acknowledged for providing synchrotron radiation and technical support. This work was partially funded by the Deutsche Forschungsgemeinschaft (TO 169/12-1 and TO 169/14-1), the Bundesministerium für Bildung und Forschung (05 KSPE1 and 05 KSPEA), the Deutscher Akademischer Auslandsdienst (313-PPP-SF-08-Ik and 1127504), the Research Funds of the University of Helsinki, and the Academy of Finland (1127462, Centers of Excellence Program 2006-2011, NGSMP).

■ REFERENCES

(1) Sloan, E.; Koh, C. *Clathrate Hydrates of Natural Gases*; CRC Press: Boca Raton, FL, 2008.
(2) Sloan, E. *Nature* **2003**, *426*, 353–359.
(3) Florusse, L.; Peters, C.; Schoonman, J.; Hester, K.; Koh, C.; Dec, S.; Marsh, K.; Sloan, E. *Science* **2004**, *306*, 469–471.
(4) Lee, H.; Lee, J.-W.; Kim, D.; Park, J.; Seo, Y.-T.; Zeng, H.; Moudrakovski, I.; Ratcliffe, C.; Ripmeester, J. *Nature* **2005**, *434*, 743–746.
(5) Sugahara, T.; Haag, J.; Warntjes, A.; Prasad, P.; Sloan, E.; Koh, C.; Sum, A. *J. Phys. Chem. C* **2010**, *114*, 15218–15222.
(6) Makino, T.; Sugahara, T.; Ohgaki, K. *J. Chem. Eng. Data* **2005**, *50*, 2058–2060.
(7) Leaist, D.; Murray, J.; Post, M.; Davidson, D. *J. Phys. Chem.* **1982**, *86*, 4175–4178.
(8) Tombari, E.; Presto, S.; Salvetti, G.; Johari, G. *J. Chem. Phys.* **2006**, *124*, 154507.
(9) Park, Y.; Choi, Y.; Yeon, S.; Lee, H. *J. Phys. Chem. B* **2008**, *112*, 6897–6899.
(10) Alavi, S.; Susilo, R.; Ripmeester, J. *J. Chem. Phys.* **2009**, *130*, 174501.
(11) Alavi, S.; Udachin, K.; Ripmeester, J. *Chem.—Eur. J.* **2010**, *16*, 1017.
(12) Lehmkühler, F.; Sakko, A.; Sternemann, C.; Hakala, M.; Nygård, K.; Sahle, C.; Galambosi, S.; Steinke, I.; Tiemeyer, S.; Nyrow, A.; Buslaps, T.; Pontoni, D.; Tolan, M.; Hämäläinen, K. *J. Phys. Chem. Lett.* **2010**, *1*, 2832–2836.
(13) Conrad, H.; Lehmkühler, F.; Sternemann, C.; Sakko, A.; Paschek, D.; Simonelli, L.; Huotari, S.; O., F.; Tolan, M.; Hämäläinen, K. *Phys. Rev. Lett.* **2009**, *103*, 218301.
(14) Radhakrishnan, R.; Trout, B. *J. Chem. Phys.* **2002**, *117*, 1786–1796.
(15) Hawtin, R.; Quigley, D.; Rodger, P. *Phys. Chem. Chem. Phys.* **2008**, *10*, 4853–4864.
(16) Walsh, M.; C.A., K.; Sloan, E.; Sum, A.; Wu, D. *Science* **2009**, *326*, 1095–1098.
(17) Jacobson, L.; Hujo, W.; Molinero, V. *J. Am. Chem. Soc.* **2010**, *132*, 11806–11811.
(18) Vatamanu, J.; Kusalik, P. *Phys. Chem. Chem. Phys.* **2010**, *12*, 15065–15072.
(19) Lehmkühler, F.; Paulus, M.; Sternemann, C.; Lietz, D.; Venturini, F.; Gutt, C.; Tolan, M. *J. Am. Chem. Soc.* **2009**, *131*, 585.
(20) Schülke, W. *Electron Dynamics by Inelastic X-ray Scattering*; Oxford University Press: Oxford, U.K., 2008.
(21) Cooper, M.; Mijnarends, P.; Shiotani, N.; Sakai, N.; Bansil, A. *X-ray Compton Scattering*; Oxford University Press: Oxford, U.K., 2004.
(22) Isaacs, E.; Shukla, A.; Platzman, P.; Hamann, D.; Barbiellini, B.; Tulk, C. *Phys. Rev. Lett.* **1999**, *82*, 600–603.
(23) Hakala, M.; Nygård, K.; Manninen, S.; Pettersson, L.; Hämäläinen, K. *Phys. Rev. B* **2006**, *73*, 035432.
(24) Hakala, M.; Nygård, K.; Manninen, S.; Huotari, S.; Buslaps, T.; Nilsson, A.; Pettersson, L.; Hämäläinen, K. *J. Chem. Phys.* **2006**, *125*, 084504.
(25) Sit, P.-L.; Bellin, C.; Barbiellini, B.; Testemale, D.; Hazemann, J.-L.; Buslaps, T.; Marzari, N.; Shukla, A. *Phys. Rev. B* **2007**, *76*, 245413.
(26) Nygård, K.; Hakala, M.; Manninen, S.; Itou, M.; Sakurai, Y.; Hämäläinen, K. *Phys. Rev. Lett.* **2007**, *99*, 197401.
(27) Barbiellini, B.; Bellin, C.; Loupias, G.; Buslaps, T.; Shukla, A. *Phys. Rev. B* **2009**, *79*, 155115.
(28) Bellin, C.; Barbiellini, B.; Klotz, S.; Buslaps, T.; Rousse, T.; Straessle, G.; Shukla, A. *Phys. Rev. B* **2011**, *83*, 094117.
(29) Sternemann, C.; Huotari, S.; Hakala, M.; Paulus, M.; Volmer, M.; Gutt, C.; Buslaps, T.; Hiraoka, N.; Klug, D.; Hämäläinen, K.; Tolan, M.; Tse, J. *Phys. Rev. B* **2006**, *73*, 195104.
(30) Volmer, M.; Sternemann, C.; Tse, J.; Buslaps, T.; Hiraoka, N.; Bull, C.; Gryko, J.; McMillan, P.; Paulus, M.; Tolan, M. *Phys. Rev. B* **2007**, *76*, 195104.
(31) Krisch, M.; Sette, F.; Masciovecchio, C.; Verbeni, R. *Phys. Rev. Lett.* **1997**, *78*, 2843–2846.
(32) Hämäläinen, K.; Manninen, S. *J. Phys.: Condens. Matter* **2001**, *13*, 7539–7556.
(33) Bergmann, U.; Glatzel, P.; Cramer, S. *Microchem. J.* **2002**, *71*, 221–230.
(34) Sternemann, C.; Sternemann, H.; Huotari, S.; Lehmkühler, F.; Tolan, M.; Tse, J. *J. Anal. At. Spectrom.* **2008**, *23*, 807–813.
(35) Wernet, P.; Nordlund, D.; Bergmann, U.; Ogasawara, H.; Cavalleri, M.; Näslund, L.; Hirsch, T.; Ojamae, L.; Glatzel, P.; Odelius, M.; Pettersson, L.; Nilsson, A. *Science* **2004**, *304*, 995–999.
(36) Cai, Y. Q.; Mao, H.-K.; Chow, P. C.; Tse, J. S.; Ma, Y.; Patchkovskii, S.; Shu, J. F.; Struzhkin, V.; Hemley, R. J.; Ishii, H.; Chen, C. C.; Jarrige, I.; Chen, C. T.; Shieh, S. R.; Huang, E. P.; Kao, C. C. *Phys. Rev. Lett.* **2005**, *94*, 025502.
(37) Tse, J. S.; Shaw, D. M.; Klug, D. D.; Patchkovskii, S.; Vankó, G.; Monaco, G.; Krisch, M. *Phys. Rev. Lett.* **2008**, *100*, 095502.
(38) Pylkkänen, T.; Giordano, V.; Chervin, J.; Sakko, A.; Hakala, M.; Soininen, J. A.; Hämäläinen, K.; Monaco, G.; Huotari, S. *J. Phys. Chem. B* **2010**, *114*, 3804–3808.
(39) Hiraoka, N.; Buslaps, T.; Honkimäki, V.; Suortti, P. *J. Synchrotron Radiat.* **2005**, *12*, 670–674.
(40) Conrad, H.; Lehmkühler, F.; Sternemann, C.; O., F.; Simonelli, L.; Huotari, S.; Tolan, M. *Rev. Sci. Instrum.* **2009**, *80*, 026103.
(41) Holm, P. *Phys. Rev. A* **1988**, *37*, 3706–3719.
(42) Verbeni, R.; Pylkkänen, T.; Huotari, S.; Simonelli, L.; Vankó, G.; Martel, K.; Henriquet, C.; Monaco, G. *J. Synchrotron Radiat.* **2009**, *16*, 469–476.
(43) Sternemann, H.; Sternemann, C.; Seidler, G.; Fister, T.; Sakko, A.; Tolan, M. *J. Synchrotron Radiat.* **2008**, *15*, 162–169.
(44) Hermann, K.; Pettersson, L. G. M.; Casida, M. E.; Daul, C.; Goursot, A.; Koester, A.; Proynov, E.; St-Amant, A.; Salahub, D. R.; Carravetta, V.; Duarte, H.; Friedrich, C.; Godbout, N.; Guan, J.; Jamorski, C.; Leboeuf, M.; Leetmaa, M.; Nyberg, M.; Patchkovskii, S.; Pedocchi, L.; Sim, F.; Triguero, L.; Vela, A. *StoBe-deMon*, version 3.0; 2009, http://www.rz-berlin.mpg.de/~hermann/StoBe/StoBeMAN.html.
(45) Jones, C.; Marshall, S.; Chakoumakos, B.; Rawn, C.; Ishii, Y. *J. Phys. Chem. B* **2003**, *107*, 6026–6031.
(46) Sakko, A.; Hakala, M.; Soininen, J. A.; Hämäläinen, K. *Phys. Rev. B* **2007**, *76*, 205115.
(47) Steiner, T.; Saenger, W. *Acta Crystallogr., B* **1994**, *50*, 348–357.
(48) Bieze, T.; van der Maarel, J.; Leyte, J. *Chem. Phys. Lett.* **1993**, *216*, 56–62.
(49) Nygård, K.; Hakala, M.; Manninen, S.; Andrejczuk, A.; Itou, M.; Sakurai, Y.; Pettersson, L.; Hämäläinen, K. *Phys. Rev. E* **2006**, *74*, 031503.
(50) Lehtola, J.; Hakala, M.; Vaara, J.; Hämäläinen, K. *Phys. Chem. Chem. Phys.* **2011**, *13*, 5630–5641.
(51) Pylkkänen, T.; Sakko, A.; Hakala, M.; Hämäläinen, K.; Monaco, G.; Huotari, S. *J. Phys. Chem. B* **2011**, to be published.
(52) Sakko, A.; Galambosi, S.; Inkinen, J.; Pylkkänen, T.; Hakala, M.; Huotari, S.; Hämäläinen, K. *Phys. Chem. Chem. Phys.* **2011**, *13*, 11678–11685.
(53) Alavi, S.; Ripmeester, J.; Klug, D. *J. Chem. Phys.* **2006**, *124*, 014704.
(54) Nowaczyk, A.; Geil, B.; Schildmann, S.; Böhmer, R. *Phys. Rev. B* **2009**, *80*, 144303.